UNIVERSITY
OF TRENTO

DIPARTIMENTO DI INGEGNERIA E SCIENZA DELL'INFORMAZIONE

38123 Povo – Trento (Italy), Via Sommarive 14
http://www.disi.unitn.it

ITERATIVE MULTI-RESOLUTION RETRIEVAL OF NON-MEASUREBLE EQUIVALENT CURRENTS FOR IMAGING OF DIELECTRIC OBJECTS

P. Rocca, M. Donelli, G. L. Gragnani, and A. Massa

May 2009

Technical Report # DISI-11-029

Iterative Multi-Resolution Retrieval of Non-Measurable Equivalent Currents for Imaging of Dielectric Objects

P. Rocca[1], M. Donelli[1], G. L. Gragnani[2], and A. Massa[1]

[1] Department of Information Engineering and Computer Science, *ELEDIA* Research Group, University of Trento, Via Sommarive 14, 38050 Trento - Italy, Tel. +39 0461 882057, Fax. +39 0461 882093

[2] Department of Biophysical and Electronic Engineering, University of Genoa, Via Opera Pia 11/A, 16145 Genoa - Italy, Tel. +39 010 3532244, Fax +39 010 3532245

E-mail: *paolo.rocca@disi.unitn.it, massimo.donelli@disi.unitn.it, gragnani@dibe.unige.it, andrea.massa@ing.unitn.it*

Abstract. In this paper, an iterative multi-resolution method for the reconstruction of the unmeasured components of the equivalent current density is proposed in order to improve the retrieval of the dielectric properties of an unknown scenario probed by interrogating electromagnetic waves. The mathematical formulation, concerned with lossless as well as lossy dielectric scatterers, is provided and the theory is supported by a set of representative examples dealing with synthetic as well as experimental scattering data.

Key Words **-** Inverse scattering, Non-measurable currents, Iterative multi-scaling method.

Classification Numbers (MSC) - 45Q05, 78A46, 78M50

1. Introduction

In the framework of electromagnetic data inversion, several methodologies consider the introduction of an equivalent current density defined into the dielectric domain in order to linearize the scattering equations [1][2][3][4]. One of the main drawbacks of these approaches lies in the non-uniqueness of the arising inverse source problem [5] and,

consequently, how to properly take into account the so-called "*non-radiating*" (or "*non-measurable*" when the electromagnetic data are measured only in a limited domain or positions outside the investigation domain) components of the unknown equivalent source. Failing to do so usually causes an inaccurate retrieval of the scatterer profile, which, in many realistic cases, suffers from a strong low-pass effect [1][2].

In order to overcome this drawback, *Habashy et al.* [6] proposed a reconstruction method where the problem of non-measurable currents was properly and directly addressed by means of an iterative algorithm that proceeds through the minimization of two cost functions. At the initial step the scattering data are matched through the reconstruction of the radiating or minimum norm scattering currents, then subsequent steps refine the non-radiating scattering and the material properties inside the scatterer.

Taking into account these guidelines, *Gragnani and Caorsi* [7] proposed a nonlinear procedure. Starting from the reconstruction of the measurable current components, carried out through a singular value decomposition (SVD) of the discretized Green's operator, the problem was recast as the solution of a nonlinear set of equations where the unknowns are the non-measurable components as well as the dielectric properties of the investigation domain. Although the obtained results indicated a significant improvement compared to those obtained through the minimum-norm solution, the method showed some inaccuracies due to the trade-off between achievable spatial-resolution and the dimension of the non-radiating currents space. As a matter of fact, the existence of non-radiating currents causes the non-uniqueness of the the inverse source problem (i.e., determining the current defined in the investigation domain that radiates an assigned electromagnetic field in the observation domain) and the corresponding presence of a non-empty null space of the integral scattering operator [8][9]. Moreover, since a numerically-accurate discretization of the integral scattering operators requires a detailed representation of the equivalent sources characterized by a sampling beyond the Nyquist rate, the resultant set of algebraic equations is generally undetermined and the arising impedance matrix turns out to be non-square with a null-space of large dimension. Therefore, a rough current description with a smaller number of basis functions decreases the size of the null space, but it yields an inaccurate spatial accuracy in the reconstruction. On the other hand, the problem becomes harder to solve when a more detailed representation is adopted due to the non-uniqueness of the solution.

In this paper, starting from the idea that an inverse source method may yield

a reasonable reconstruction of the scatterer under test when the number of degrees of freedom to model the object is small [10], an iterative multi-zooming process is adopted. By keeping at each iteration of the zooming process the number of unknowns close to the number of independent data collectable from the field measurements [11], it is possible on one hand to fully exploit the reduction of the null-space for restoring the well-position of the inverse problem and, on the other hand, to enhance the achievable spatial resolution thus avoiding low-detailed reconstructions [10]. More specifically, starting from a coarse representation of the unknowns, the method iteratively defines a subgridding of the support of the equivalent current density successively improving the representation (in terms of spatial accuracy) of the current as well as the scatterer profile of lossless and lossy dielectric objects by minimizing a suitable nonlinear multi-resolution cost function.

An outline of the paper is as follows. The mathematical issues concerned with the proposed approach are detailed in Section 2, while Section 3 is devoted to a preliminary numerical assessment. A set of representative test cases are dealt with and analyzed by comparing the obtained results with those from the homogeneous-resolution method [7] (in the following, indicated as "*bare*" approach) as well as the minimum-norm solution. Moreover, some comparisons with an alternative $IMSA$-based approach [12] are discussed. Eventually, in Section 4, some conclusions are drawn.

2. Mathematical Formulation

Let us consider a two-dimensional inverse scattering problem under TM plane wave illumination. By considering a set of V illuminations, $\underline{E}^v_{inc}(\underline{r}) = E^v_{inc}(x,y)\,\hat{z}\; v = 1, ..., V$, probing an unknown investigation domain D_{inv} described through the following contrast function

$$\tau(x,y) = [\varepsilon_R(x,y) - 1] - j\frac{\sigma(x,y)}{\omega\varepsilon_0}\ , \tag{1}$$

(ε_R and σ being the relative permittivity and conductivity, respectively; ε_0 is the dielectric permittivity of the lossless and non-magnetic background) the arising electromagnetic scattering phenomena turn out to be described by the *Data* and *State* integral equations that in the contrast-source formulation appear as follows

$$E^v_{scat}(x,y) = -j\frac{k_0^2}{4}\int\int_{D_{inv}} J^v_{eq}(x',y')\,H_0^{(2)}(k_0 d)\,dx'dy' \qquad (x,y)\in D_{obs} \tag{2}$$

$$\tau(x,y)\,E^v_{inc}(x,y) = J^v_{eq}(x,y) + j\frac{k_0^2}{4}\tau(x,y)\int\int_{D_{inv}} J^v_{eq}(x',y')\,H_0^{(2)}(k_0 d)\,dx'dy' \qquad (x,y)\in D_{inv} \tag{3}$$

where

$$J_{eq}^{v}(x,y) = \tau(x,y)\, E_{tot}^{v}(x,y)\,; \quad v = 1,\ldots,V \tag{4}$$

$k_0 = \frac{2\pi}{\lambda}$, λ being the wavelength of the free-space background medium and $H_0^{(2)}$ is the 0-th order second-kind Hankel function $[d = \sqrt{(x-x')^2 + (y-y')^2}]$.

Starting from the measurement of a set of $M^{(v)}$ $(v = 1, ..., V)$ samples of the scattered electric field, $E_{scat}^{v}(x,y)$, collected in an external observation domain D_{obs} and of the knowledge of the incident field in the investigation domain, the inversion process is aimed at determining $\tau(x,y)$ and $J_{eq}^{v}(x,y)$ in the investigation domain through the inversion of (2)(3). Towards this end, the iterative multi-scaling strategy $(IMSA-NR)$ is adopted where a multi-resolution representation of the unknowns is taken into account at each step s of the reconstruction process

$$\tau(x,y) = \sum_{r=1}^{R(s)} \sum_{n(r)=1}^{N(r)} \tau\left(x_{n(r)}, y_{n(r)}\right) B_{n(r)}(x,y) \tag{5}$$

$$J_{eq}^{v}(x,y) = \sum_{r=1}^{R(s)} \sum_{n(r)=1}^{N(r)} c_{n(r)}^{v} V_{n(r)}^{v}(x,y) \tag{6}$$

where $\left\{B_{n(r)}(x,y)\,;\, n(r) = 1, ..., N(r)\right\}$ is a set of rectangular basis functions, r and $N(r)$ being the spatial-resolution index and the number of basis functions at the r-th level, respectively. Moreover, $\left\{V_{n(r)}^{v}(x,y)\,;\, n(r) = 1, ..., N(r)\right\}$ defines an orthonormal set of eigenvectors computed by means of the SVD of the discretized external Green's operator G_{ext} [7], which turns out being equal to

$$G_{ext}^{v}(x,y) = \sum_{m=1}^{M^{(v)}} \sum_{n(r)=1}^{N(r)} U_{m}^{v}(x,y)\, \alpha_{n(r)}^{v} \left[V_{n(r)}^{v}(x,y)\right]^{*}. \tag{7}$$

According to such a description, the problem unknowns are the contrast coefficients $\left\{\tau\left(x_{n(r)}, y_{n(r)}\right)\,;\, n(r) = 1, ..., N(r);\, r = 1, ..., R(s)\right\}$ and the non-radiating source components $\left\{c_{n(r)}^{v} = \zeta_{n(r)}^{v};\, n(r) = I(r)+1, ..., N(r);\, r = 1, ..., R(s)\right\}$, since the remaining source coefficients (namely, the minimum norm components, $\left\{c_{n(r)}^{v} = \xi_{n(r)}^{v};\, n(r) = 1, ..., I(r);\, r = 1, ..., R(s)\right\}$ are easily computed as follows

$$\xi_{n(r)}^{v} = \frac{1}{\alpha_{n(r)}^{v}} \left\{ \sum_{m=1}^{M^{(v)}} \left[U_{m}^{v}(x,y)\right]^{*} E_{scat}^{v}(x_m, y_m) \right\} \tag{8}$$

where $\left\{U_{m}^{v}(x,y)\,;\, m = 1, ..., M^{(v)}\right\}$ is another set of orthonormal eigenvectors from (7) and $\left\{\alpha_{n(r)}^{v};\, n(r) = 1, ..., I(r)\right\}$ is the corresponding set of singular values. Moreover,

the apex $*$ stands for complex conjugate. These unknowns are then determined through a multi-step procedure, where the following operations take place:

- *Zero-order Reconstruction* $(s = 0)$
  At the first iteration, the region of interest (RoI) coincides with D_{inv} $(D_{RoI}^{(0)} = D_{inv})$. Obtain a coarse reconstruction of both the contrast $\tau(x_n, y_n)$, $n = 1, ..., N$, and the induced equivalent currents $J_{eq}^{v}(x_n, y_n)$, $n = 1, ..., N$, $v = 1, ..., V$, by subdividing the RoI into N uniform cells according to the amount of information collected from the scattered field measurement [11] and solving the problem as in [7];
- *Higher-order Reconstructions* $(s \geq 1)$
  After the 0-th order reconstruction, the synthetic zoom is iteratively performed inside $D_{RoI}^{(s-1)}$ to focus the reconstruction on the support where the unknown scatterers are supposed to be located. More in detail,
  - *Regions-of-Interest* $(RoI\text{s})$ *Estimation*
    Increase the step counter $(s \rightarrow s{+}1)$. Starting from the reconstruction obtained at the previous step (s), define the number $Q^{(s)}$, the locations $(x_{c(q)}^{(s)},\ y_{c(q)}^{(s)},\ q = 1, \ldots, Q^{(s)})$, and the extensions $(L_{(q)}^{(s)},\ q = 1, \ldots, Q^{(s)})$ of the regions-of-interest $D_{RoI(q)}^{(s)}$ (where the $Q^{(s)}$ scatterers are supposed to be located) according to the *clustering procedure* described in [12] and perform a noise filtering to eliminate some artifacts in the reconstructed image [13];
  - *Initialization*
    In the RoIs, set the currents to the minimum norm solution $[c_{n(r)}^{v} = \xi_{n(r)}^{v}$, $n(r) = 1, ..., I(r)$ and $\zeta_{n(r)}^{v} = 0.0$, $n(r) = I(r) + 1, ..., N(r)$, being $r = R(s)]$ as well as the object function $[\tau_{guess}^{(s)}\left(x_{n(r)}, y_{n(r)}\right) = \tau_{MN}^{(s)}\left(x_{n(r)}, y_{n(r)}\right)]$, where

$$\tau_{MN}^{(s)}\left(x_{n(r)}, y_{n(r)}\right) = \frac{1}{V}\sum_{v=1}^{V}\left\{\frac{J_{MN}^{v}\left(x_{n(r)}, y_{n(r)}\right)}{E_{tot_{MN}}^{v}\left(x_{n(r)}, y_{n(r)}\right)}\right\} \tag{9}$$

    being $E_{tot_{MN}}^{v}(x, y)$ the field generated in the RoIs when the scatterer is modeled by means of the minimum-norm equivalent source $J_{MN}^{v}(x, y) = \sum_{r=1}^{R(s)}\sum_{n(r)=1}^{I(r)}\xi_{n(r)}^{v}V_{n(r)}^{v}(x, y)]$. More specifically,

$$\begin{aligned} E_{tot_{MN}}^{v}\left(x_{n(r)}, y_{n(r)}\right) &= E_{inc}^{v}\left(x_{n(r)}, y_{n(r)}\right) + \\ &+ \sum_{u(r)=1}^{N(r)} J_{MN}^{v}\left(x_{u(r)}, y_{u(r)}\right) G_{2d}^{v}\left(A_{u(r)}, d_{u(r),n(r)}\right) \end{aligned} \tag{10}$$

    G_{2d}^{v} and $A_{u(r)}$ being the discretized form of the Green's operator and the area

of the u-th cell at the r-th resolution level, respectively;

– *Unknowns Retrieval*

Determine a new estimate of the unknowns $\{\tau_{(q)}^{(s)}\left(x_{n(r)}, y_{n(r)}\right);\ n(r) = 1, ..., N(r), r = 1, ..., R(s)\}$ and $\{\zeta_{n(r)}^{v},\ n(r) = I(r)+1, ..., N(r), r = 1, ..., R(s)\}$ through the minimization of the multi-resolution cost function

$$\Phi_{IMSA-NR}^{(s)} = \frac{\Gamma^{(s)}}{\sum_{q=1}^{Q^{(s)}} \sum_{v=1}^{V} \sum_{r=1}^{R(s)} \sum_{n(r)=1}^{I(r)} \left\{ w_{n(r)}^{(q)} \left| \xi_{n(r)}^{v} V_{n(r)}^{v}\left(x_{n(r)}, y_{n(r)}\right)\right|^2 \right\}} \tag{11}$$

$\Gamma^{(s)}$ being the residual defined as

$$\begin{aligned}\Gamma^{(s)} = \sum_{q=1}^{Q^{(s)}} \sum_{v=1}^{V} \sum_{r=1}^{R(s)} \sum_{n(r)=1}^{N(r)} \Big\{ & w_{n(r)}^{(q)} \left| \tau_{(q)}^{(s)}\left(x_{n(r)}, y_{n(r)}\right) E_{inc}^{v}\left(x_{n(r)}, y_{n(r)}\right) + \right. \\ & - \left[\sum_{j(r)=1}^{I(r)} \xi_{j(r)}^{v} V_{j(r)}^{v}\left(x_{n(r)}, y_{n(r)}\right) + \sum_{j(r)=I(r)+1}^{N(r)} \zeta_{n(r)}^{v} V_{j(r)}^{v}\left(x_{n(r)}, y_{n(r)}\right) \right] + \\ & + \tau_{(q)}^{(s)}\left(x_{n(r)}, y_{n(r)}\right) \sum_{u(r)=1}^{N(r)} \left[\sum_{j(r)=1}^{I(r)} \xi_{j(r)}^{v} V_{j(r)}^{v}\left(x_{u(r)}, y_{u(r)}\right) + \right. \\ & \left. \left. + \sum_{j(r)=I(r)+1}^{N(r)} \zeta_{n(r)}^{v} V_{j(r)}^{v}\left(x_{u(r)}, y_{u(r)}\right) \right] G_{2d}\left(A_{u(r)}, d_{u(r),n(r)}\right) \right|^2 \Big\} \end{aligned} \tag{12}$$

where w is a weighting function

$$w_{n(r)}^{(q)} = \begin{cases} 0 & if\ \left(x_{n(r)}, y_{n(r)}\right) \notin D_{RoI(q)}^{(s-1)} \\ 1 & if\ \left(x_{n(r)}, y_{n(r)}\right) \in D_{RoI(q)}^{(s-1)} \end{cases}; \tag{13}$$

– *Convergence Check*

Go to the "*RoIs Estimation*" until a stationary condition [12] either on the number of *RoI*s

$$\frac{1}{s} \sum_{\gamma=1}^{s} \left\{ \left| Q^{(s)} - Q^{(\gamma)} \right| \right\} \leq \eta_q \tag{14}$$

or on the qualitative reconstruction parameters

$$\min_{q=1,...,Q^{(s)}} \left\{ \frac{\left| u_{(q)}^{(s)} - u_{(q)}^{(s-1)} \right|}{\left| u_{(q)}^{(s)} \right|} \times 100 \right\} < \eta_u, \quad u = x_c,\ y_c,\ L \tag{15}$$

holds true ($s = S_{opt}$), η_q and η_u being fixed thresholds.

3. Numerical Validation

In order to test the effectiveness of the proposed approach and also to evaluate the benefit respect to the "*bare*" approach, some numerical simulations have been

performed by considering synthetic as well as experimental scattering data where field data are collected for both lossless as well as lossy dielectric objects. Moreover, some reconstructions concerned with inhomogeneous objects are compared with those obtained by means of another implementation of the same multi-resolution strategy that, unlike the NR-based approach at hand, exploits the contrast-field (CF) formulation of the scattering equations (2)-(3).

Figure 1 shows the actual geometry of the first model on which we tested the $IMSA-NR$. The scatterer is a lossless homogeneous ($\tau^{ref}=1.0$) circular cylinder of radius $R=\frac{\lambda}{6}$ centered at $x_C^{ref}=y_C^{ref}=0.15\,\lambda$ and located in a square investigation domain λ-sided. By considering such a scenario, synthetic scattering data have been generated with a MoM simulator (partitioning D_{inv} in $N_{MoM}=100\times100$ homogeneous square sub-domains) using $V=4$ illuminations and $M^{(v)}=8$, $v=1,...,V$, measurement locations in a circular observation domain ($R_{D_{obs}}=0.74\,\lambda$). Moreover, the samples of $E^v_{scat}(x_m,y_m)$, $m=1,...,M^{(v)}$, $v=1,...,V$, have been blurred with a Gaussian noise characterized by different values of signal-to-noise ratio (SNR) in order to assess the robustness of the approach. The reconstruction results obtained by minimizing the cost function (11) through the alternate conjugate gradient method [14] are shown in Figs. 2-3 ($SNR=10\,dB$) and Figs. 4-5 ($SNR=5\,dB$) in terms of both dielectric profile and equivalent current density [i.e., $J_{eq}(x,y)=\frac{\sum_{v=1}^{V}J^v_{eq}(x,y)}{V}$]. The $IMSA-NR$-based inversion has been carried out by discretizing $D^{(s)}_{RoI}$ in $N(r)=10\times10$, $r=R(s)$ square sub-domains. For comparison, the minimum-norm solution and that obtained with the "*bare*" approach [7] are also shown (D_{inv} discretized into $N=20\times20$ in order to have a spatial resolution of the same order as that of the $IMSA-NR$ in the RoI where the actual scatterer is located). As it can be observed, whatever the SNR value, a non-negligible improvement is obtained when using the iterative multi-scaling procedure. As a matter of fact, by comparing the retrieved distributions [Fig. 2(c) and Fig. 3(c) - $SNR=10\,dB$; Fig. 4(c) and Fig. 5(c) - $SNR=5\,dB$] with the actual profiles [Fig. 2(d) and Fig. 3(d)], it turns out that the $IMSA-NR$ performs better as confirmed by the error indexes defined as follows

$$\Xi^{\tau}_{(j)}=\sum_{r=1}^{R}\frac{1}{N^{(j)}_{(r)}}\sum_{n(r)=1}^{N^{(j)}_{(r)}}\left\{\frac{\left|\tau^{(S_{opt})}\left(x_{n(r)},y_{n(r)}\right)-\tau^{ref}\left(x_{n(r)},y_{n(r)}\right)\right|}{\left|\tau^{ref}\left(x_{n(r)},y_{n(r)}\right)\right|}\right\}\times100 \quad (16)$$

where $N^{(j)}_{(r)}$ ranges over the whole investigation domain ($j\Rightarrow tot$), or over the area where the actual object is located ($j\Rightarrow int$), or over the background belonging to the

investigation domain ($j \Rightarrow ext$),

$$\delta = \frac{\sqrt{\left[x_C^{(S_{opt})} - x_C^{ref}\right]^2 + \left[y_C^{(S_{opt})} - y_C^{ref}\right]^2}}{\lambda} \tag{17}$$

$$\Delta = \left\{ \frac{L^{(S_{opt})} - L^{ref}}{L^{ref}} \right\} \times 100 \tag{18}$$

and reported in Tab. I.

The second test case is concerned with a set of data experimentally-acquired in a controlled environment at the Institute Fresnel, Marseille, France [15]. The experimental set-up consisted of a fixed emitter (a double-ridged horn transmitting antenna) and the object has been illuminated from $V = 36$ different locations equally-spaced on a circle $R_{D_{obs}} = 720\,mm \pm 3\,mm$ in radius. Due to the physical limitations, the scattered field has been measured in $M^{(v)} = 49$ points for each illumination angle from a receiver rotating, with a mechanical support, around the vertical axis of scatterer under test. A detailed description of the underlying experimental setup together with the complete data-set can be found in the introduction of [16] (pp. 1565-1571) by Belkebir and Saillard. As far as the scattering configuration is concerned, two different experiments with lossless as well as lossy objects are considered. In the former case, the multiple-objects scenario called "*twodielTM_ 8f.exp*" illuminated by the probing source at a working frequency of $f = 3\,GHz$ has been managed. More in detail, the scatterers are two lossless homogeneous dielectric cylinders characterized by an object function $\tau_{(1)}^{ref} = \tau_{(2)}^{ref} = 2.0 \pm 0.3$ with circular cross-sections $R = 0.15\,\lambda$ in radius and placed about $0.3\,\lambda$ from the center of the experimental setup. The latter experiment deals with the "*rectTM_ dece.exp*" dataset, where an off-centered highly conducting cylinder of rectangular section of $0.17\,\lambda \times 0.34\,\lambda$ is illuminated by an impinging wave at the frequency of $f = 4\,GHz$. In both the experiments, the objects have been supposed to lie in a square area of $30\,cm \times 30\,cm$ (i.e., $3\,\lambda \times 3\,\lambda$ when $f = 3\,GHz$, and $4\,\lambda \times 4\,\lambda$ when $f = 4\,GHz$). The retrieved profiles are shown in Fig. 6 and Fig. 8‡, respectively. As expected, thus confirming the conclusions drawn in the first example, the reconstruction with the $IMSA - NR$ [Fig. 6(c), Fig. 8(c)] is much closer to the actual cylinder compared

‡ Because of the highly conducting assumption on the scatterer properties, the *a-priori* condition $Re\{\tau(x,y)\}$ has been made.

to the "*bare*" solution [Fig. $6(b)$, Fig. $8(b)$] where the scatterers are only localized. Moreover, the reported results demonstrate that the proposed inverse algorithm can work effectively when dealing with complex scenarios, where either multiple objects, or small loss type of scatterers are embedded in the region under test. For completeness, Figure 7 and Figure 9 reports the inversion results in terms of current densities.

Finally, the reconstruction of inhomogeneous objects is taken into account to further assess the effectiveness of the $IMSA-NR$ approach. In these experiments, the results of the $IMSA-NR$ are compared with those of both the "bare" approach and the $IMSA-CG$ [17] where, unlike (2) and (3), the inverse scattering equations are expressed in terms of the dielectric profile and the induced electric field instead of contrast and source distributions. The scattered field data have been experimentally-acquired at the same laboratory of the previous experimental dataset [18]. The same investigation domain D_{inv} has been kept, while the acquisition setup differs in terms of radius of the measurement domain (i.e., $R_{D_{obs}} = 167\,cm$), number of views, and number of measurement points. As regards to the data-sets called "*FoamDielExtTM*" and "*FoamDielIntTM*", $V = 8$ and $M^{(v)} = 241$. Two different objects having radius equal to $R_1 = 80\,mm$ and $R_2 = 30\,mm$ and estimated dielectric properties $\tau_{(1)}^{ref} = 0.45 + j0.0$ and $\tau_{(2)}^{ref} = 2.0 + j0.0$ are under test in both scenarios. In the former case ("*FoamDielExtTM*"), the objects are placed one close to the other, while the small scatterer is located inside the bigger one in the "*FoamDielIntTM*" scenario.

The images of the reconstructed dielectric profiles for both test cases are shown in Fig. 10 ($f = 2\,GHz$) and Fig. 11 ($f = 4\,GHz$), respectively. They are concerned with the solutions obtained with the "*bare*" approach [Figs. $10(a)$-$11(a)$], the $IMSA-NR$ [Figs. $10(b)$-$11(b)$] and the $IMSA-CG$ [Figs. $10(c)$-$11(c)$]. Also in such a numerical assessment, is worth noticing that the $IMSA-NR$ succeeds in distinguishing and correctly localizing the two scatterers. On the contrary, the solutions from the "*bare*" approach present some artifacts [Fig. $10(a)$] and a low-pass representation of the actual profile [Fig. $11(a)$], respectively.

As far as the $IMSA-CG$ is concerned, the retrieved profiles are quite similar to those obtained by $IMSA-NR$ approach thus pointing out the efficiency and reliability of the multi-zooming strategy for dealing with inverse scattering problems. Nevertheless, it is worthwhile to observe that the quality of the $IMSA-NR$ reconstructions is slightly better than that of the $IMSA-CG$ ones. As a matter of fact, both scatterers turn out to be more carefully defined in Fig. $10(b)$ and Fig. $11(b)$ than in Fig. $10(c)$ and Fig.

11(c), respectively. Such an event is mainly related to the attempt of the NR technique of exploiting the information on the scatterer coming from the non-radiating parts of the induced equivalent sources. Otherwise, the CF approach of the $IMSA-CG$ only considers the amount of information coming from the scattered field, which is related to the measurable component of the equivalent source (i.e., J^v_{MN}).

4. Conclusions

In this paper, the $IMSA-NR$ has been described. The iterative method proceeds by improving at each step a multi-resolution representation of both the object function and the equivalent current density in the investigation domain. At each step, the scattered data are initially matched through the solution of an inverse source problem for the minimum-norm part of the scattering currents. Then, the process updates the material properties and the non-radiating part of the equivalent currents in order to minimize a suitable multi-resolution cost function.

A preliminary evaluation of the effectiveness of the $IMSA-NR$ in dealing with noisy as well as experimental data has been carried out pointing out a significant improvement with respect to single-step approaches for the reconstruction of non-measurable currents. Moreover, some comparisons with an alternative CF formulation of the $IMSA$ strategy have pointed out that it is profitable to exploit the knowledge of the existence of the null-space of the inverse scattering operators. Certainly, several issues still need to be addressed, but, thanks to these experiments, it may be stated that globally the approach demonstrated an acceptable stability and robustness to noisy conditions allowing, also in the presence of large errors in the scattering data, an accurate localization and reconstruction of lossless as well as lossy scatterers under test.

References

[1] M. M. Ney, A. M. Smith, and S. S. Stuchly, "A solution of electromagnetic imaging using pseudoinverse transformation," *IEEE Trans. Med. Imag.*, vol. 3, pp. 155-162, 1984.

[2] S. Caorsi, G. L. Gragnani, and M. Pastorino, "Equivalent current density reconstruction for microwave imaging reconstruction," *IEEE Trans. Microwave Theory Tech.*, vol. 37, no. 5, pp. 910-916, May 1989.

[3] T. M. Habashy, E. Y. Chow, and D. G. Dudley, "Profile inversion using the renormalized source-type integral equation approach," *IEEE Trans. Antennas Propagat.*, vol. 38, no. 5, pp. 668-681, May 1990.

[4] S. Caorsi, G. L. Gragnani, and M. Pastorino, "A multiview microwave imaging system for two-dimensional penetrable objects," *IEEE Trans. Microwave Theory Tech.*, vol. 39, no. 5, pp. 845-851, May 1991.

[5] N. Bleistein and J. K. Cohen, "Nonuniqueness in the inverse source problem in acoustics and electromagnetics," *J. Math. Phys. N. Y.*, vol. 18, no. 2, pp. 194-201, Feb. 1977.

[6] T. M. Habashy, M. L. Oristaglio and A. T. de Hoop, "Simultaneous nonlinear reconstruction of two-dimensional permittivity and conductivity," *Radio Science*, vol. 29, no. 4, pp. 1101-1118, Jul.-Aug. 1994.

[7] S. Caorsi, and G. L. Gragnani, "Inverse-scattering method for dielectric objects based on the reconstruction of the nonmeasurable equivalent current density," *Radio Science*, vol. 34, no. 1, pp. 1-8, 1999.

[8] A. J. Devaney and E. Wolf, "Radiating and nonradiating classical current distributions and the fields they generate," *Phys. Rev. D Part. Fields*, vol. 8, no. 4, pp. 1044-1047, Aug. 1973.

[9] G. Gbur, "Nonradiating sources and the inverse source problem," Ph.D. Thesis, Dept. of Physics and Astronomy, University of Rochester, Rochester, N.Y., 2001.

[10] W. C. Chew, Y. M. Wang, G. Otto, D. Lesselier and J. C. Bolomey, "On the inverse source method of solving inverse scattering problems," *Inverse Problems*, vol. 10, pp. 547-553, 1994.

[11] O. M. Bucci and G. Franceschetti, "On the degrees of freedom of scattered fields," *IEEE Trans. Antennas Propagat.*, vol. 37, no. 7, pp. 918-926, Jul. 1989.

[12] S Caorsi, M. Donelli, and A. Massa, "Detection, location, and imaging of multiple scatterers by means of the iterative multiscaling method," *IEEE Trans. Microwave Theory Tech.*, vol. 52, pp. 1217-1228, Apr. 2004.

[13] S. Caorsi, M. Donelli, and A. Massa, "Analysis of the stability and robustness of the iterative multiscaling approach for microwave imaging applications," *Radio Sci.*, vol. 39, RS5008, pp. 1-17, Oct. 2004.

[14] R. E. Kleinmann and P. M. Van den Berg, " A modified gradient method for two-dimensional problems in tomography," *J. Comput. Appl. Math.*, vol. 42, pp. 17-35, 1992.

[15] K. Belkebir, S. Bonnard, F. Sabouroux, and M. Saillard, "Validation of 2D inverse scattering algorithms from multi-frequency experimental data," *J. Electromagn. Waves Appl.*, vol. 14, pp. 1637-1668, Dec. 2000.

[16] K. Belkebir and M. Saillard, "Testing inversion algorithm against experimental data," *Inverse Problems*, vol. 17, pp. 1565-1571, Dec. 2001.

[17] M. Donelli, D. Franceschini, A. Massa, M. Pastorino, and A. Zanetti, "Multi-resolution iterative inversion of real inhomogeneous targets," *Inverse Problems*, vol. 21, no. 6, pp. S51-S63, Dec. 2005.

[18] J.-M. Geffrin, P. Sabouroux, and C. Eyraud, "Free space experimental scattering database continuation: experimental set-up and measurement precision," *Inverse Problems*, vol. 21, no. 6, pp. S117-S130, Dec. 2005.

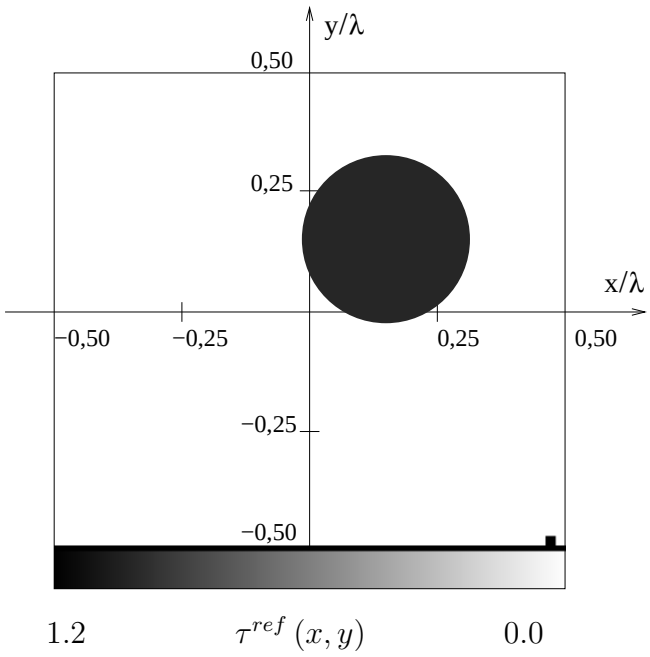

Figure 1. *Off-Centered Circular Scatterer* ($R = \frac{\lambda}{6}$, $x_C = y_C = 0.15\lambda$, $\tau = 1.0$). Reference scenario of the first numerical test case.

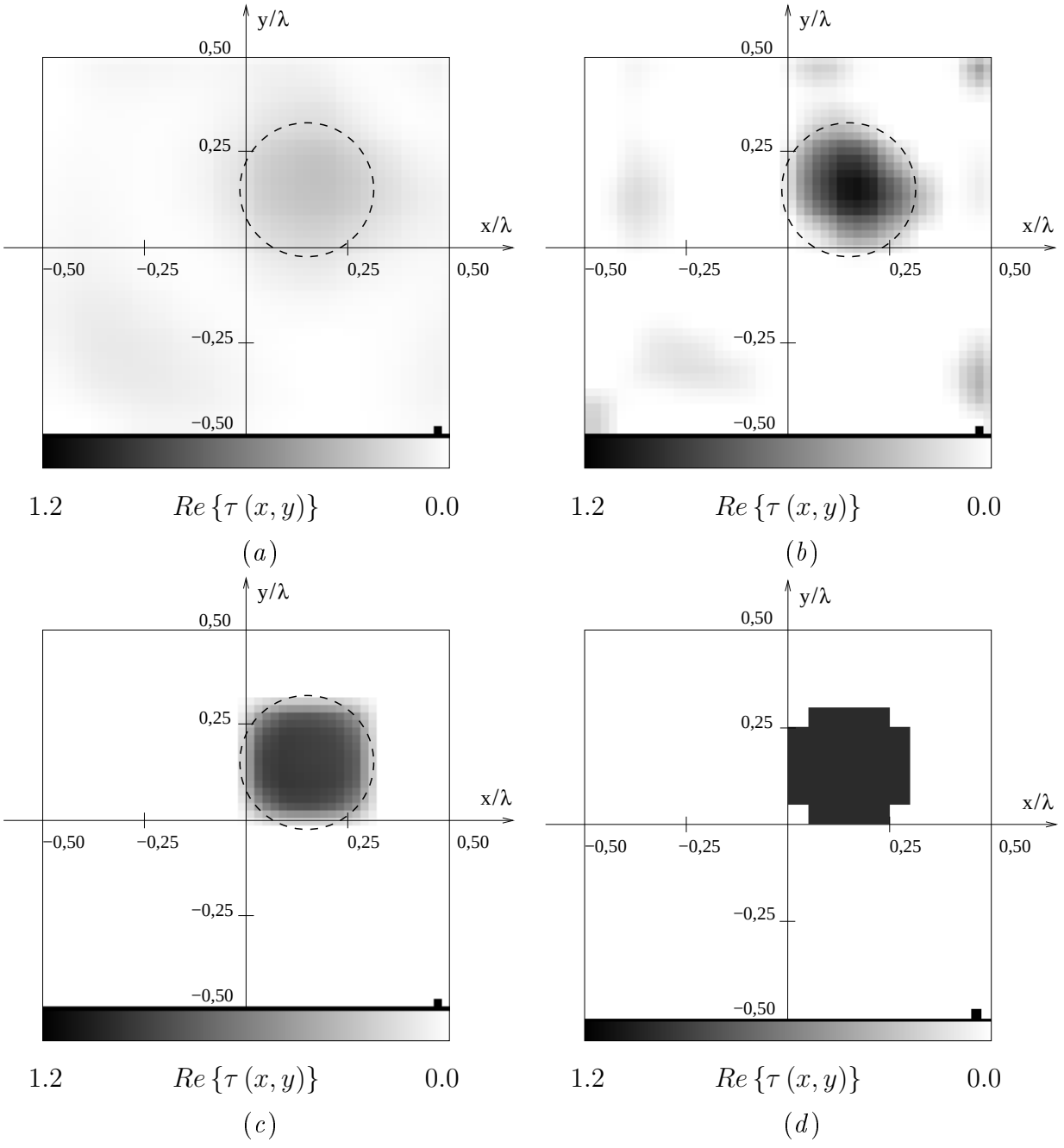

Figure 2. *Off-Centered Circular Scatterer* ($R = \frac{\lambda}{6}$, $x_C = y_C = 0.15\lambda$, $\tau = 1.0$, $V = 4$, $M^{(v)} = 8$, $SNR = 10\,dB$). *Object Function Reconstruction* - Minimum-norm solution (a). Retrieved distributions with the "*bare*" [7] procedure (b) and the $IMSA - NR$ approach [$s = S_{opt} = 4$ (c)]. Optimal reconstruction of the actual dielectric profile achievable with the $IMSA - NR$ approach (d).

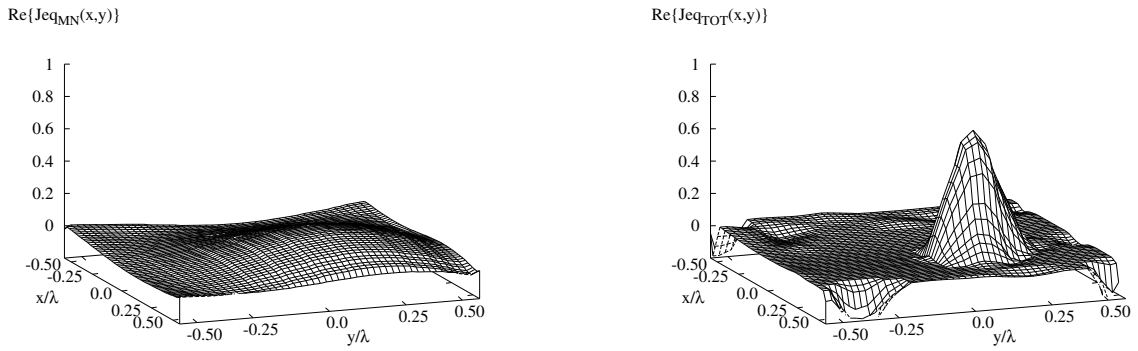

(a) (b)

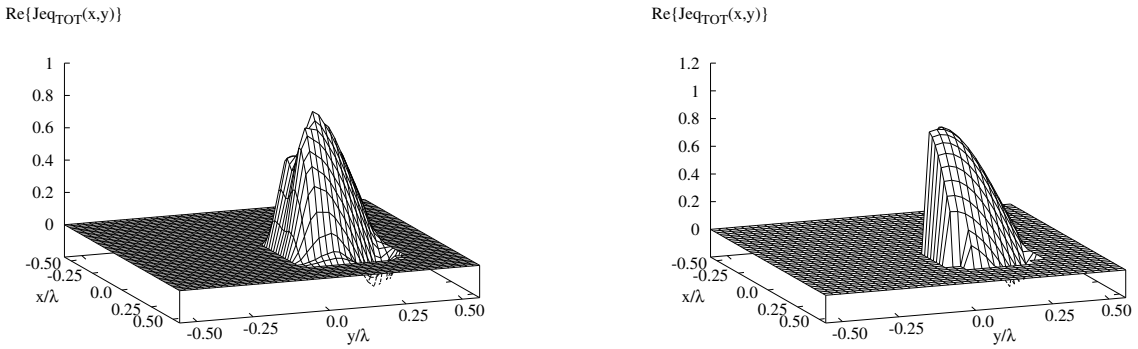

(c) (d)

Figure 3. *Off-Centered Circular Scatterer* ($R = \frac{\lambda}{6}$, $x_C = y_C = 0.15\lambda$, $\tau = 1.0$, $V = 4$, $M^{(v)} = 8$, $SNR = 10\,dB$). *Equivalent Current Density Reconstruction* - Minimum-norm solution (a). Retrieved distributions with the "*bare*" [7] procedure (b) and the $IMSA - NR$ approach $[s = S_{opt} = 4\ (c)]$. Actual current distribution $(N = 40 \times 40)$ (d).

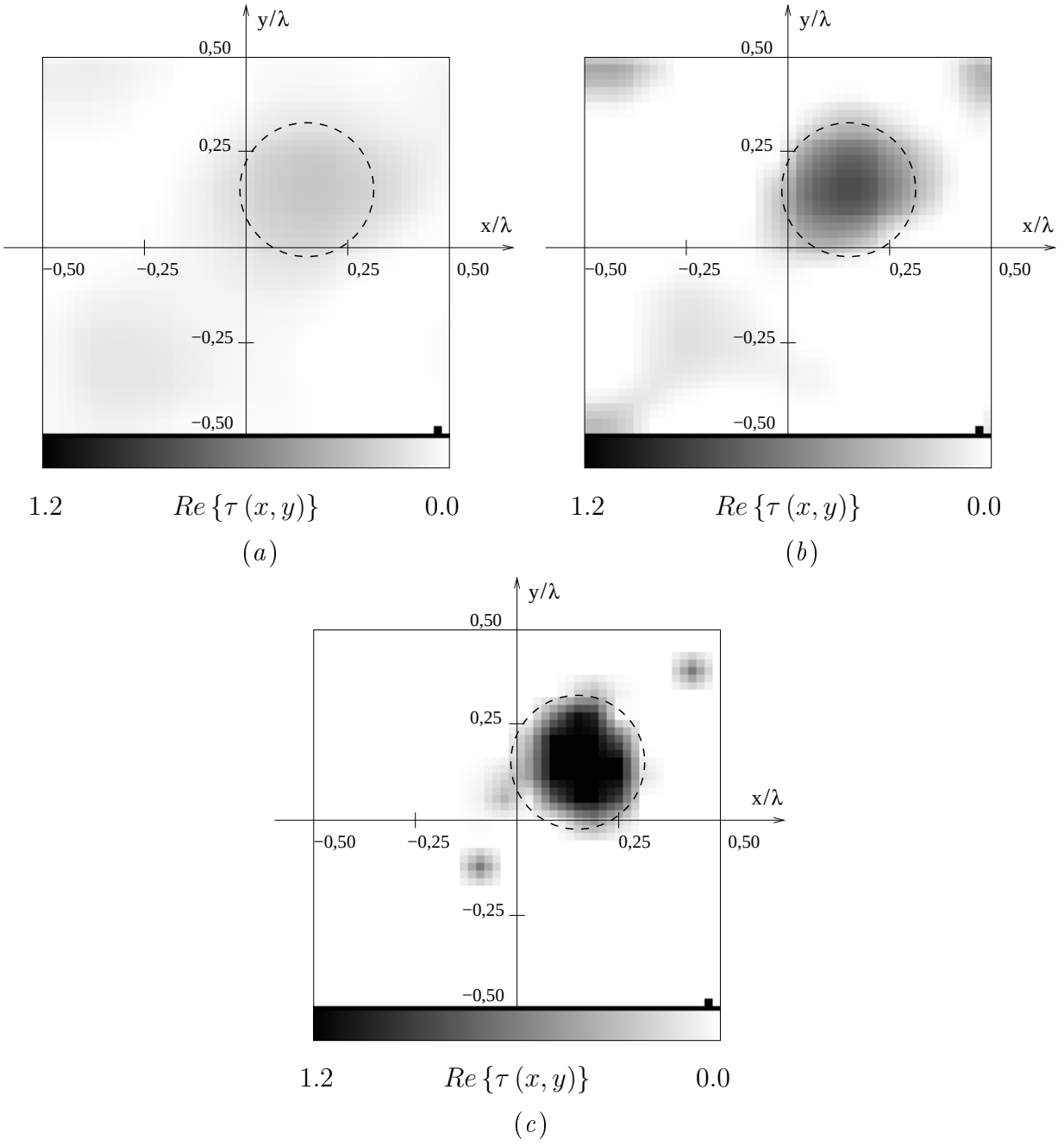

Figure 4. *Off-Centered Circular Scatterer* ($R = \frac{\lambda}{6}$, $x_C = y_C = 0.15\lambda$, $\tau = 1.0$, $V = 4$, $M^{(v)} = 8$, $SNR = 5\,dB$). *Object Function Reconstruction* - Minimum-norm solution (a). Retrieved distributions with the "*bare*" [7] procedure (b) and the $IMSA - NR$ approach $[s = S_{opt} = 2\ (c)]$.

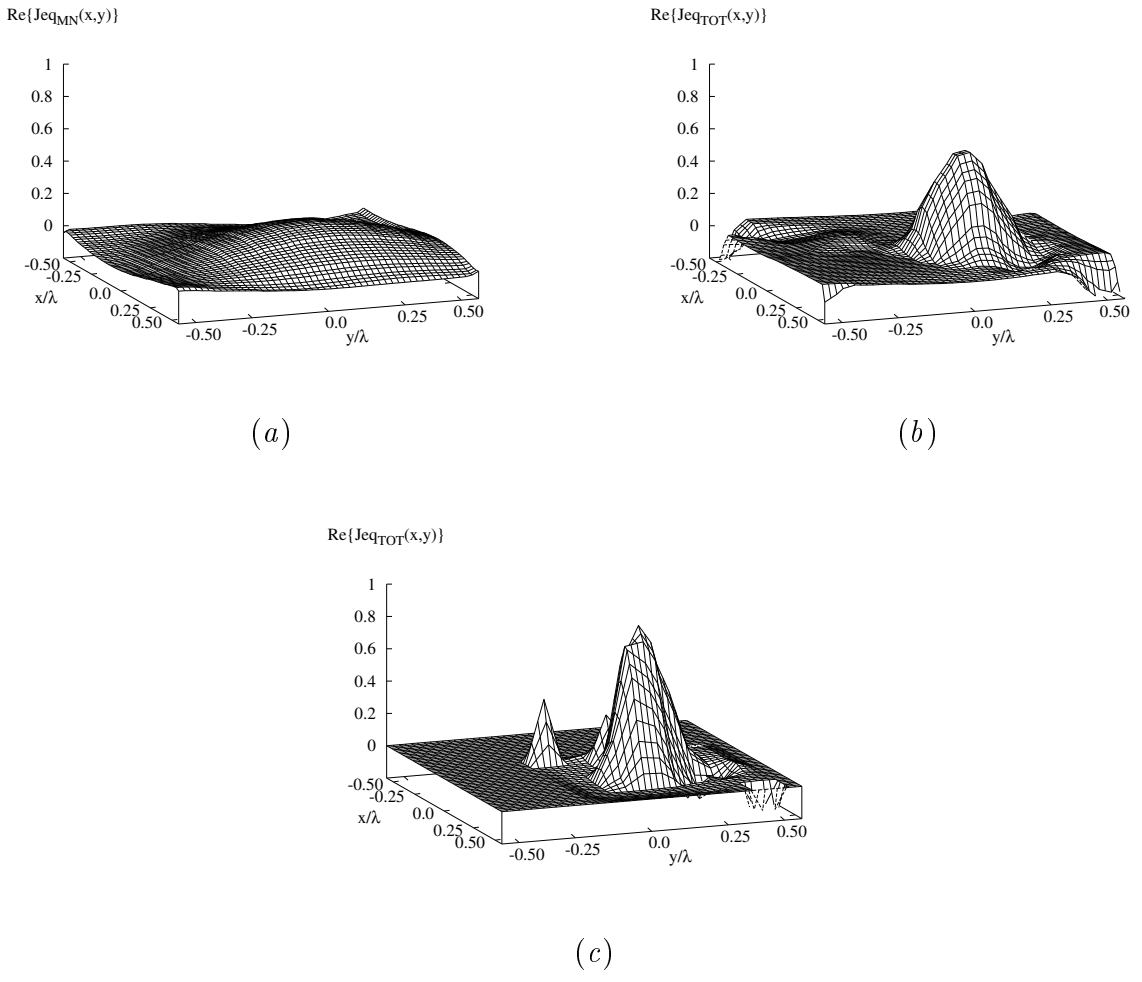

(a) (b)

(c)

Figure 5. *Off-Centered Circular Scatterer* ($R = \frac{\lambda}{6}$, $x_C = y_C = 0.15\lambda$, $\tau = 1.0$, $V = 4$, $M^{(v)} = 8$, $SNR = 5\,dB$). *Equivalent Current Density Reconstruction* - Minimum-norm solution (a). Retrieved distributions with the "*bare*" [7] procedure (b) and the $IMSA - NR$ approach $[s = S_{opt} = 2\ (c)]$.

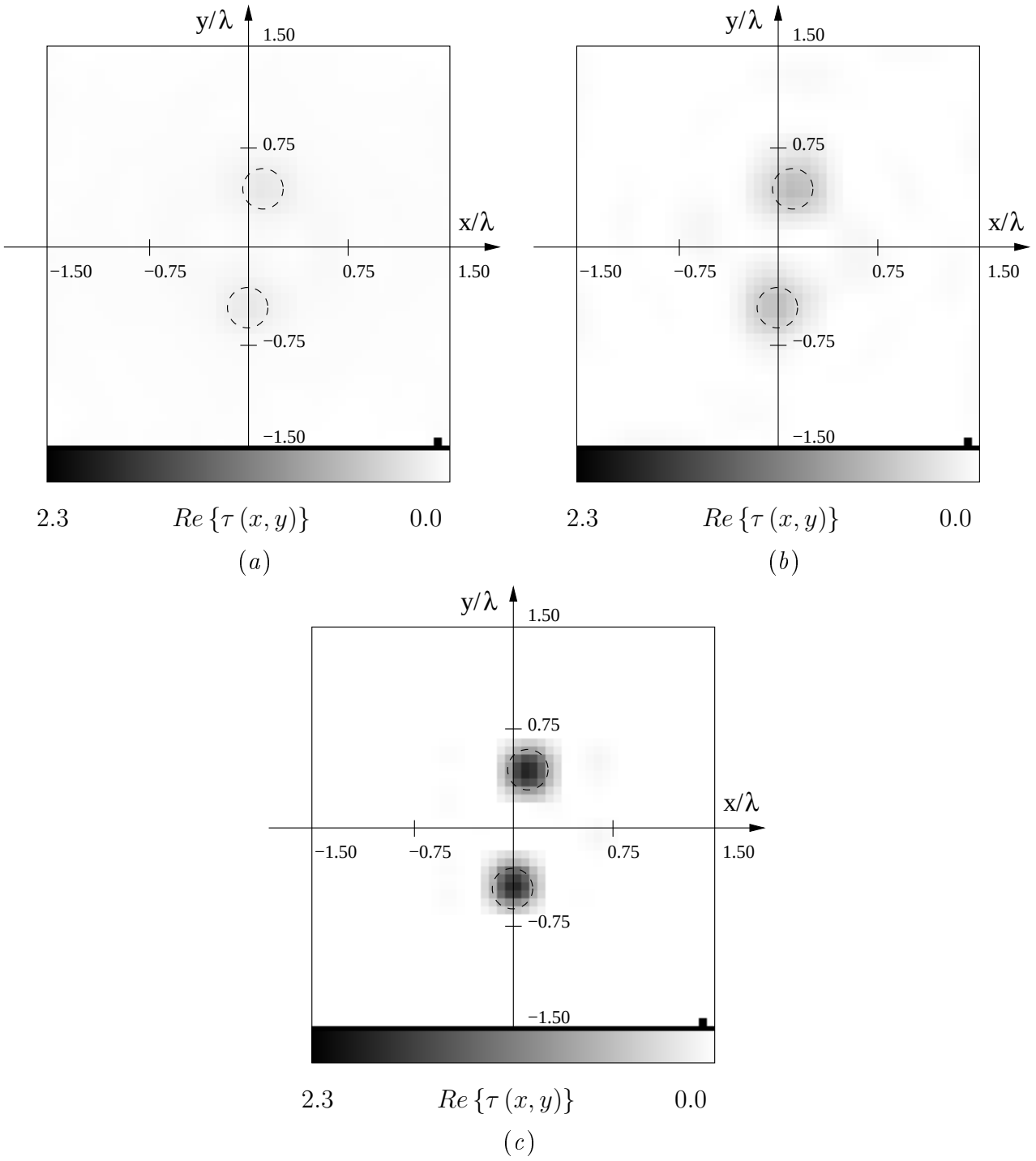

Figure 6. *Dataset "twodielTM_ 8f.exp" - Benchmark "Marseille"* [16] ($f = 3\,GHz$). *Object Function Reconstruction* - Minimum-norm solution (a). Retrieved distributions with the "*bare*" [7] procedure (b) and the $IMSA - NR$ approach [$s = S_{opt} = 5$ (c)].

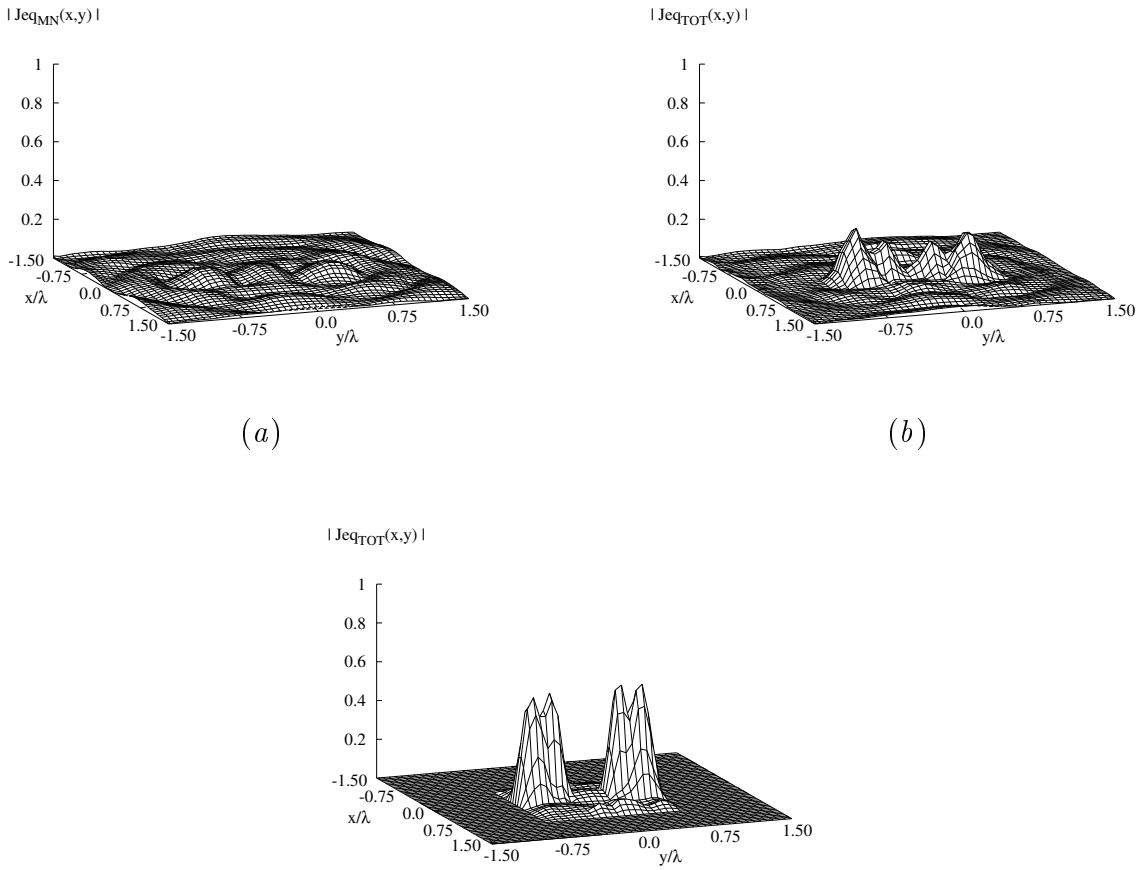

(a) (b)

(c)

Figure 7. *Dataset "twodielTM_ 8f.exp" - Benchmark "Marseille"* [16] ($f = 3\,GHz$). *Equivalent Current Density Reconstruction* - Minimum-norm solution (a). Retrieved distributions with the "*bare*" [7] procedure (b) and the $IMSA - NR$ approach $[s = S_{opt} = 5\ (c)]$.

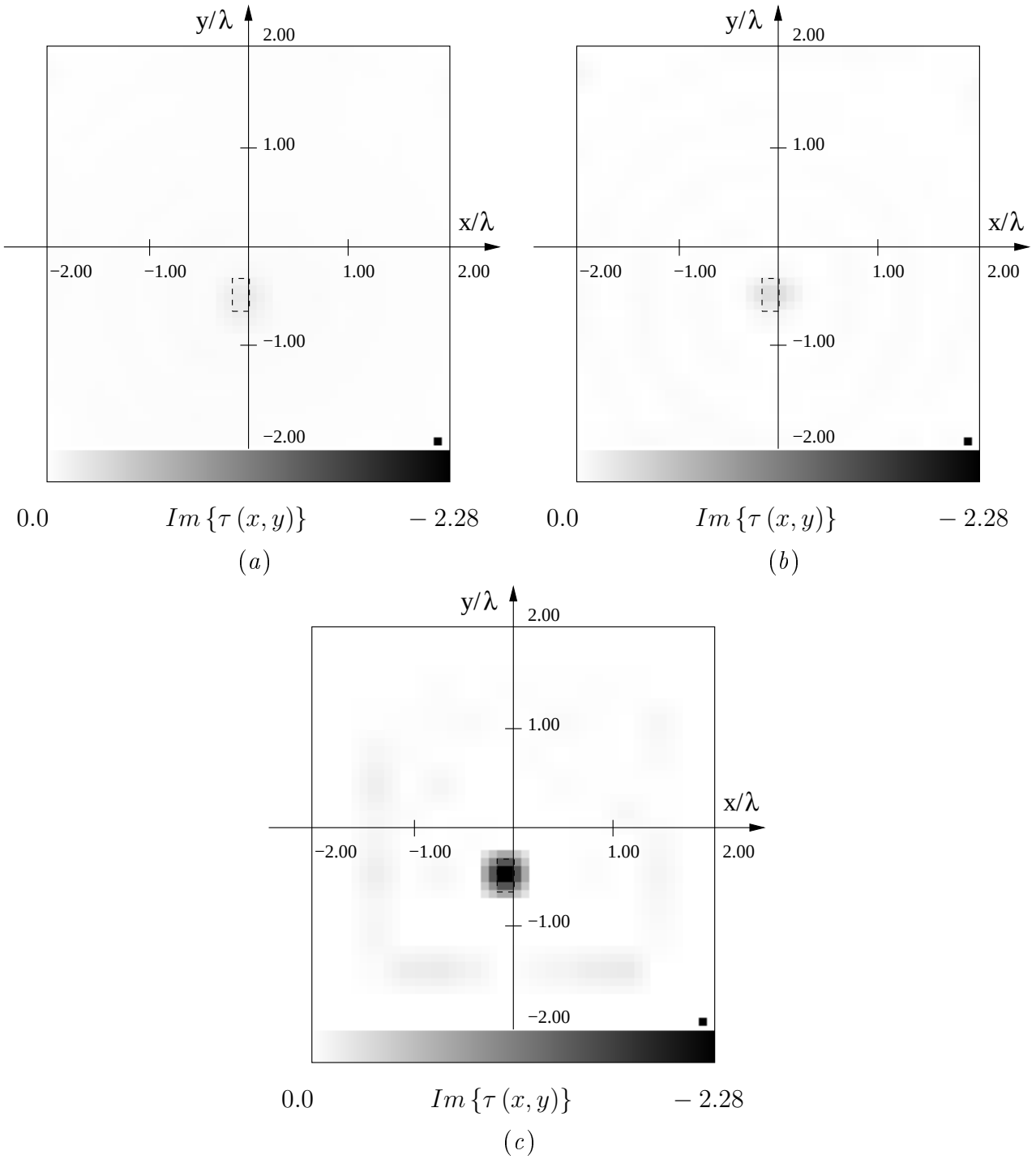

Figure 8. *Dataset "rectTM_ dece.exp" - Benchmark "Marseille"* [16] ($f = 4\,GHz$). *Object Function Reconstruction* - Minimum-norm solution (a). Retrieved distributions with the "*bare*" [7] procedure (b) and the $IMSA - NR$ approach [$s = S_{opt} = 2$ (c)].

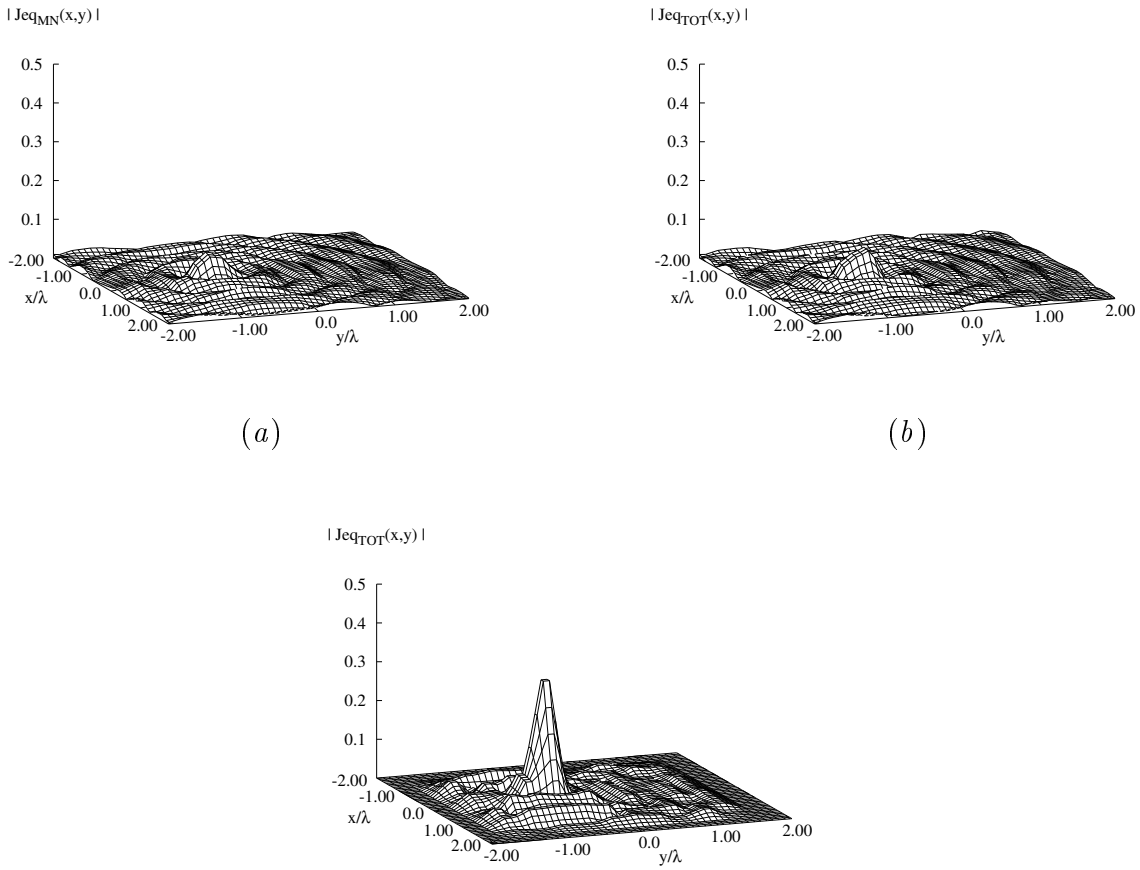

Figure 9. *Dataset "rectTM_ dece.exp" - Benchmark "Marseille"* [16] ($f = 4\,GHz$). *Equivalent Current Density Reconstruction* - Minimum-norm solution (a). Retrieved distributions with the "*bare*" [7] procedure (b) and the $IMSA - NR$ approach [$s = S_{opt} = 2$ (c)].

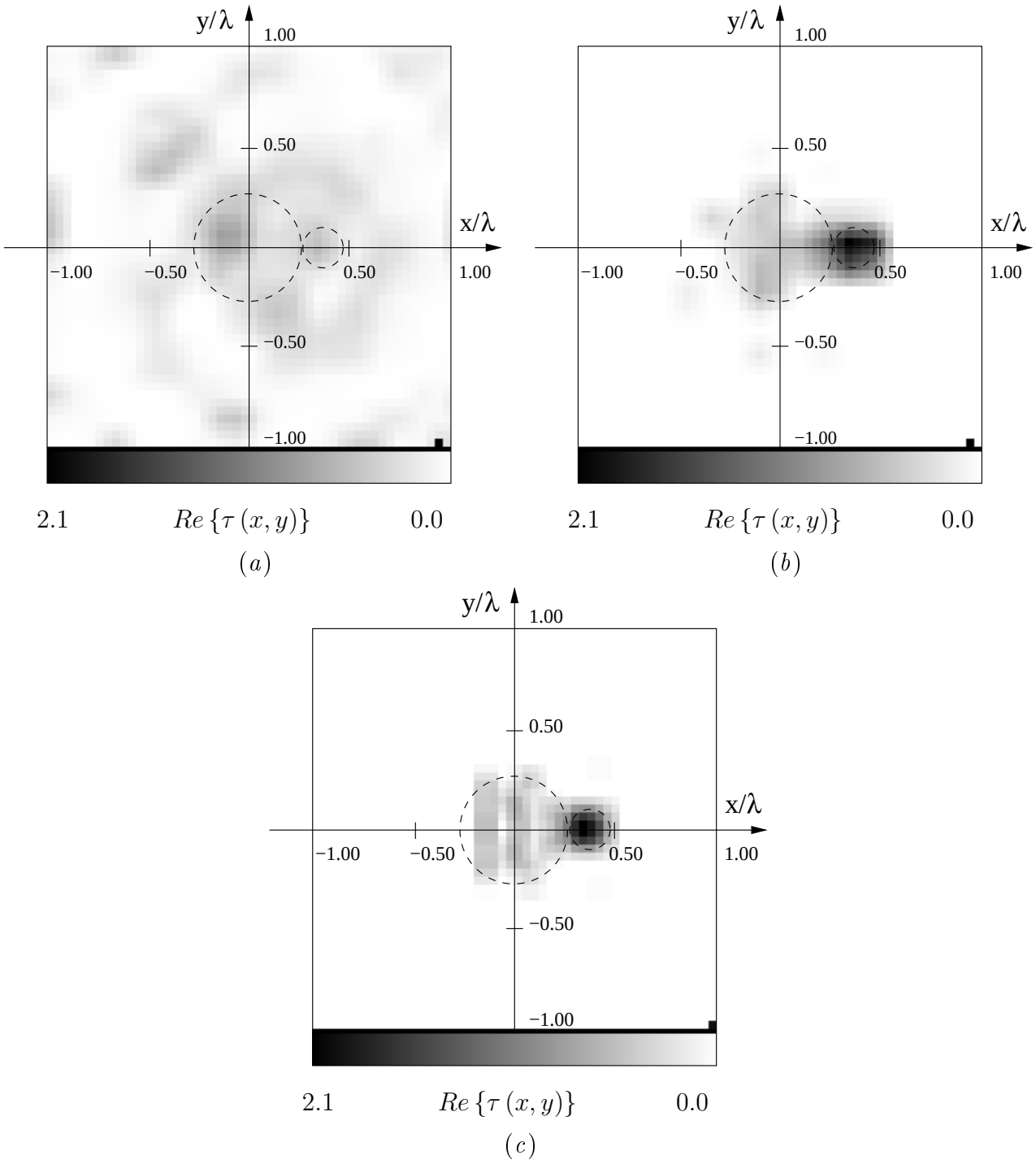

Figure 10. *Dataset "FoamDielExtTM" - Benchmark "Marseille"* [18] ($f = 2\,GHz$). *Object Function Reconstruction* - Retrieved distributions with the "*bare*" [7] procedure (a), the $IMSA - NR$ approach $[s = S_{opt} = 2]$ (b) and the $IMSA - CG$ approach $[s = S_{opt} = 2]$ (c).

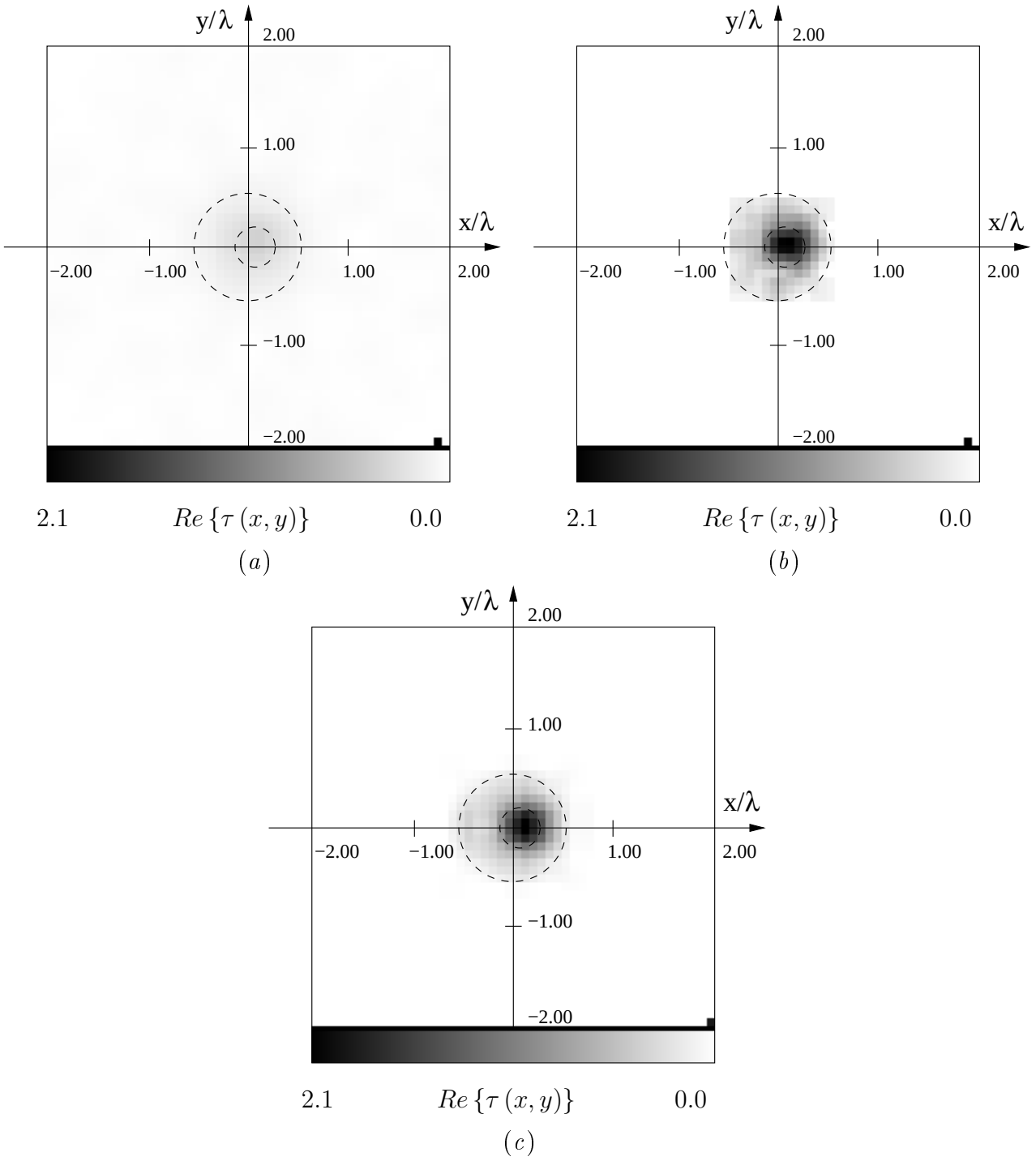

Figure 11. *Dataset "FoamDielIntTM" - Benchmark "Marseille"* [18] ($f = 4\,GHz$). *Object Function Reconstruction* - Retrieved distributions with the "*bare*" [7] procedure (a), the $IMSA - NR$ approach $[s = S_{opt} = 5]$ (b) and the $IMSA - CG$ approach $[s = S_{opt} = 2]$ (c).

	$SNR = 10\,dB$			$SNR = 5\,dB$		
	MN Solution	*Approach* [7]	$IMSA-NR$	*MN Solution*	*Approach* [7]	$IMSA-NR$
Ξ_{int}^{τ}	38.3	20.1	10.1	38.8	21.4	19.0
Ξ_{ext}^{τ}	4.42	2.45	0.26	4.25	3.75	1.29
Ξ_{tot}^{τ}	7.26	3.93	1.09	7.14	5.22	2.77
δ	1.3×10^{-1}	4.6×10^{-2}	2.8×10^{-3}	1.5×10^{-1}	9.5×10^{-3}	4.6×10^{-2}
Δ	175	93	1	171	127	25

Table I. *Off-Centered Circular Scatterer* ($R = \frac{\lambda}{8}$, $x_C = y_C = 0.15\lambda$, $\tau = 1.0$, $V = 4$, $M^{(v)} = 8$). *Object Function Reconstruction* - Values of the error indexes for the distributions retrieved with the "bare" procedure and the $IMSA-NR$ approach at different SNR.